Journal of Innovative Optical Health Sciences
Vol. 2, No. 3 (2009) 245–251

World Scientific
www.worldscientific.com

LIQUID CRYSTAL BASED ROTATING ORTHOGONAL POLARIZATION IMAGING SYSTEM

QUN ZHU, IAN M. STOCKFORD, JOHN A. CROWE and STEPHEN P. MORGAN*
School of Electrical and Electronic Engineering
University of Nottingham, University Park
Nottingham, UK NG7 2RD
**steve.morgan@nottingham.ac.uk*

Rotating orthogonal polarization imaging provides images of the polarization properties of scattering media which are free from surface reflections. Previously the technique has been demonstrated using manually rotated Glan–Thompson polarizers to control and analyze the polarization state of the light entering and emerging from the tissue. This paper describes a system that performs these functions using liquid crystal retarders. The system is tested using a polarizing target embedded within a scattering medium and is compared with Monte Carlo simulations. The results compare well with those obtained with manual rotation of polarizers. The liquid crystal based approach has advantages over the previous system in terms of ease of use, speed, and repeatability and is therefore an important step towards taking the technique into routine clinical use.

Keywords: Liquid crystal; polarization; orthogonal; surface reflection; scattering; tissue.

1. Introduction

Recently a technique termed rotating orthogonal polarization imaging (ROPI) has been proposed.[1,2] This technique enables imaging of the polarization properties of tissue that are free from surface reflections. As the name suggests, this is achieved through always maintaining orthogonal polarization illumination and detection. Polarization sensitivity is obtained through rotating the illumination and detection polarization states.

There are several potential applications of such an approach. Many tissues have polarization properties that affect the polarization state of light such as linear dichroism in sickled red blood cells: when they become deoxygenated, it has been observed[3,4] that there is different absorption depending on the polarization state of the illumination. Other polarization effects that have been observed in tissue include linear birefringence in collagen[5] and chiral rotation in glucose.[6] Applications also exist in monitoring tissue growth in bioreactors in tissue engineering.[5]

The difficulty in performing polarization difference imaging (i.e., polarized light illumination and subtraction of the co- and cross-polarized detections) of tissue is that the co-polar channel is often dominated by surface reflections. Several methods have been proposed to overcome this problem,[7–9] however, ROPI has advantages in terms of not involving the use of matching fluid, being noncontact, and comparatively simple to implement.

Previously[1,2] the technique has been demonstrated in manual rotation of Glan–Thompson polarizers for illumination of the sample and analysis of the detected light. This has disadvantages in terms of ease of use and displacement of the image as the polarizers are rotated. Although motorized rotation stages could be used, this is not an ideal

solution for a simple device that could be easily used in clinical practice. In the research described here a liquid crystal based approach has been implemented for providing illumination of the sample and analysis of the backscattered light. The liquid crystal based system has advantages in terms of ease of use, speed, and repeatability and is an important step towards taking the technique into routine clinical use. The incorporation of liquid crystals into polarization microscopy has been an important development in the field of microscopy. For example, the LC Polscope[10] has been demonstrated to provide results that compare well with conventional polarization microscopy and has resulted in a commercial device that has found widespread application. This paper aims to evaluate the use of liquid crystals in a ROPI system which should allow the method to become more robust and widely used.

Section 2 describes the liquid crystal based system and briefly describes the Monte Carlo model of image formation. Section 3 presents measurement results from phantom experiments and simulations. Discussions and conclusions follow in Sec. 4.

2. Experimental Setup and Monte Carlo Model

The experimental setup is shown in Fig. 1. Polarized light from a HeNe laser (power = 20 mW, $\lambda = 632.8$ nm) is focused onto a rotating ground glass diffuser and a collection lens. A liquid crystal retarder (Meadowlark Optics) and a fixed Glan–Thompson polarizer are used to control the polarization state of the illumination. Collimated light is focused via a cube beam splitter to the back focal plane of $a \times 4$, NA = 0.1 infinite conjugate microscope objective which provides nominally uniform illumination at the sample. An image of the sample is formed on the CCD camera (Hamamatsu ORCA ERII) via the objective, beam splitter, a liquid crystal linear retarder, a Glan–Thompson polarizer and a relay lens. The system has no moving parts.

The scattering sample is a cuvette (illuminated face dimensions 45 × 50 mm, depth 10 mm) filled with a suspension of polystyrene microspheres of diameter 1.4 μm and refractive index $n_p = 1.57$. The scattering medium has the following properties: scattering coefficient $\mu_s = 20\,\text{mm}^{-1}$, absorption coefficient $\mu_a = 3 \times 10^{-4}\,\text{mm}^{-1}$, mean cosine of the scattering angle $g = 0.94$, and refractive index of the medium $n_m = 1.33$. The optical properties of the medium have been obtained by following a recipe defined by Ref. 11. Briefly, this consists of obtaining the scattering cross-section σ_s of the scattering particle from Mie theory.[11] The scattering coefficient can then be obtained using the relationship $\mu_s = N\sigma_s$ where N is the number of particles per unit volume. N can be set by diluting the particles by an appropriate amount.

The method of forming images is shown in Fig. 2. The illumination and detection polarization states are always maintained orthogonal to one another. Rotating the polarization state provides sensitivity to the polarization properties of the medium. A dichroism image is formed by taking the

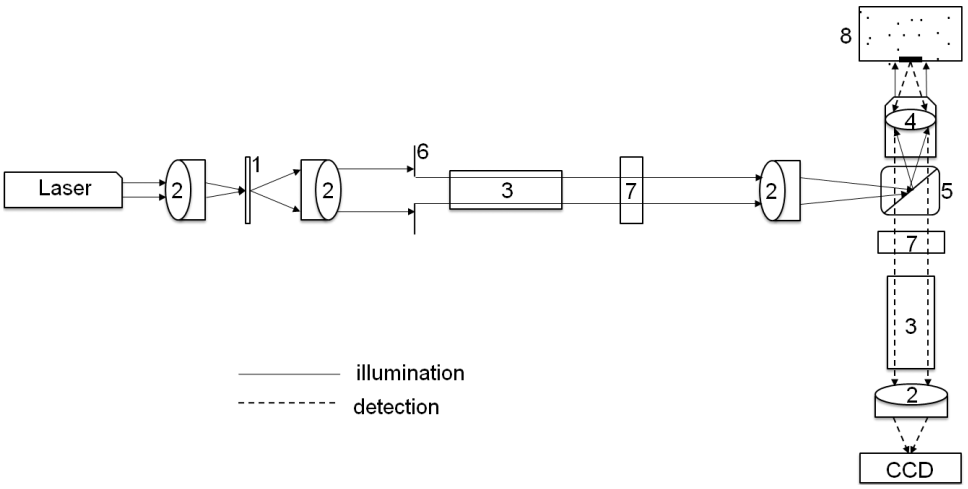

Fig. 1. ROPI experiment setup. (1) Ground glass rotating diffuser, (2) positive achromatic doublet lens, focal length = 60 mm, (3) Glan–Thompson polarizer, (4) ×4 microscope infinite conjugate objective, NA = 0.1, (5) cube beam splitter, (6) aperture, (7) liquid crystal retarder, and (8) scattering sample.

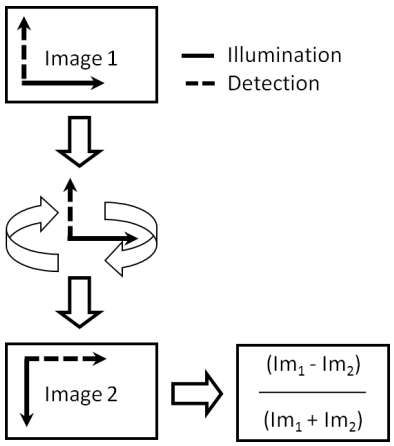

Fig. 2. Formation of images through illumination and detection in orthogonal polarization states, followed by polarization rotation and taking the difference image.

difference between two images and normalizing by the total intensity.

To evaluate the performance of the system, a 0.75 mm thick piece of sheet polarizer (8.5 × 0.85 mm) is embedded at different depths within the medium with its polarization axis vertical. As the polarization axis of the target is known (vertical), only two pairs of orthogonal polarization states ((i) vertical illumination and horizontal detection; (ii) horizontal illumination and vertical detection) are needed to measure the polarization property of the target. At least three measurements are required when the polarization axis of the target is unknown. Nonuniform illumination intensity is calibrated out by first obtaining an image of a mirror in place of the scattering medium. We have repeated the images taken in a previous publication[2] so that the performance of the new system can be compared with that of a system with conventional polarizers.

The Monte Carlo model for the full system is obtained by modifying a single point illumination, polarized light Monte Carlo model described previously.[12] The single point illumination Monte Carlo involves propagating each photon on a random walk through a scattering medium. At each scattering event, each photon has its direction modified and its Stokes vector modified by the Mueller matrix of the scattering particle. The propagation of photons continues until the photon exits the medium or exceeds a predefined distance within the medium. Different polarization states can then be resolved by the liquid crystal device upon detection by multiplying the Stokes vector of the emerging photon by the Mueller matrix of an analyzer.[13]

Three main modifications are made to the conventional single point Monte Carlo model to allow imaging to be performed (i) full field illumination, (ii) embedding a polarizing target within the scattering medium, and (iii) imaging the target plane onto a detector array. (i) is achieved through recording the coordinates when a photon crosses the target plane relative to the source. In this way different source positions can be modeled relative to the target which enables full field illumination to be built up. When applying the full field illumination method (i) we need to move the polarization target relative to the illumination source. This means that, depending on the relative position of the source and target, some photons will have interacted with the target and some will not. To be able to achieve (ii), we therefore need to record two photon paths when a photon crosses the target plane; one when the target is present at that position and the polarization state is modified and another when the target is absent and the photon polarization state is unaffected. This is a novel addition to Monte Carlo simulations of polarizing targets in scattering media. (iii) uses the position and angle when a photon emerges from the medium to calculate the position it appears to have originated from at the target plane. It is then assumed that the position at the target plane maps onto the detector plane to form an image. For the simulations shown in the next section 512 × 512 points in x and y directions are used for full field illumination, representing an area of 128 mfps × 128 mfps (mean free paths, where the mean free path is the mean distance between scattering events, $1\,\text{mfp} = 1/\mu_s$). The images are formed with 5 million photons launched into the medium with an overall detection area of 200 mfps × 200 mfps.

3. Results

Experimental images of a polarizing target embedded in a scattering medium at depths of 2, 5, 10, and 12 mfps are shown in Figs. 3 and 4. Figure 3 shows the case where the polarization axes of both illumination and target are vertical. Figure 4 shows the case where the polarization axis of the illumination is horizontal and that of the target is vertical. As described in Sec. 2, the polarization axis of the detection is always orthogonal to that of the illumination. The contrast is greater in Fig. 3 than in Fig. 4 because the target and detection polarization axes are orthogonal. Figure 5 shows the dichroism

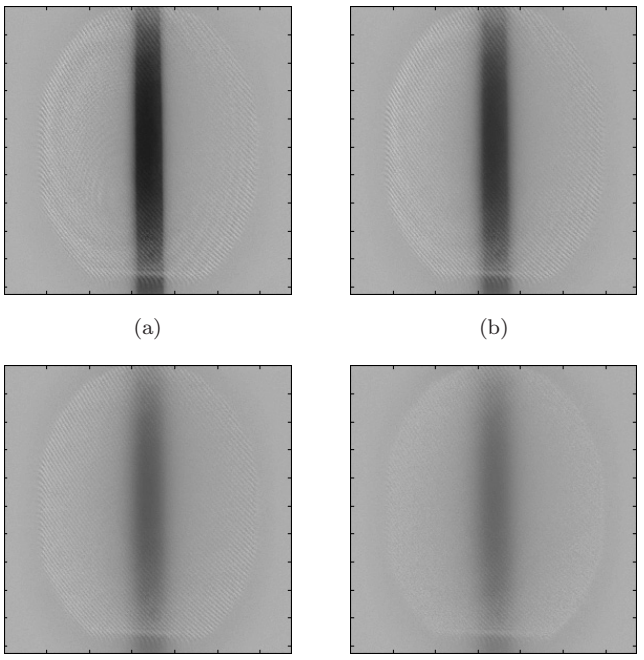

Fig. 3. Liquid crystal based experimental images of a linear polarizer located at depths of (a) 2, (b) 5, (c) 10, and (d) 12 mfps within a scattering medium. The polarization axis of the target is aligned vertically, the illumination is vertically linearly polarized with horizontal detection. Each image is 8 mm × 8 mm.

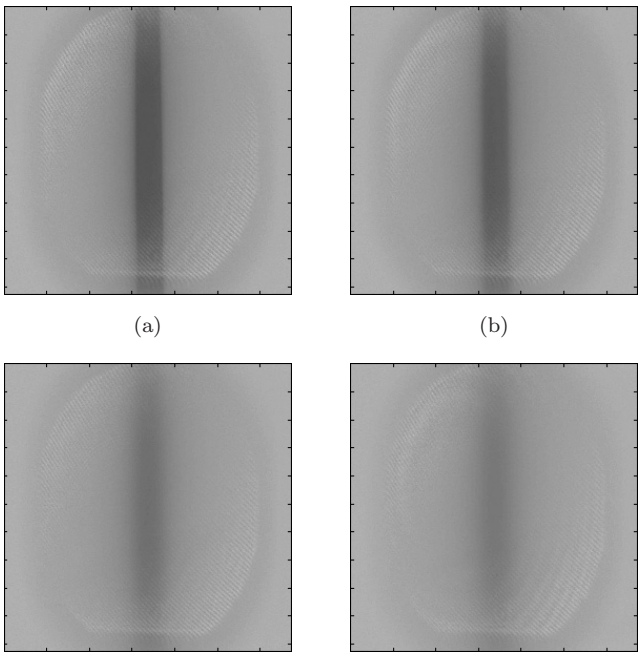

Fig. 4. Liquid crystal based experimental images of a linear polarizer located at depths of (a) 2, (b) 5, (c) 10, and (d) 12 mfps within a scattering medium. The polarization axis of the target is aligned vertically, the illumination is horizontally linearly polarized with vertical detection. Each image is 8 mm × 8 mm.

which is obtained from the normalized difference images of those in Figs. 3 and 4. The ring that can be observed in all images is due to the illumination used and the finite aperture sizes in the system. All images demonstrate a decrease in contrast with increasing object depth due to scattering occurring between the target and the surface of the scattering medium.

The experimental results have been simulated using Monte Carlo simulations. Using the medium parameters described previously, a target of width 20 mfps is embedded within the medium at depths of 2, 5, 10, and 12 mfps. The target is assumed to be infinitely long in the vertical direction and infinitesimally thin in the depth direction. The simulated images shown in Figs. 6–8 can be compared with the experimental images shown in Figs. 3–5.

Qualitatively the results of Figs. 6–8 compare well to those obtained experimentally (Figs. 3–5). All cases show that the image contrast and resolution degrades with increasing depth due to scattering. Greater contrast is observed when the polarization axis of the target is orthogonal to that of the detection (Figs. 3 and 6). Experiment and simulation are quantitatively compared over a range

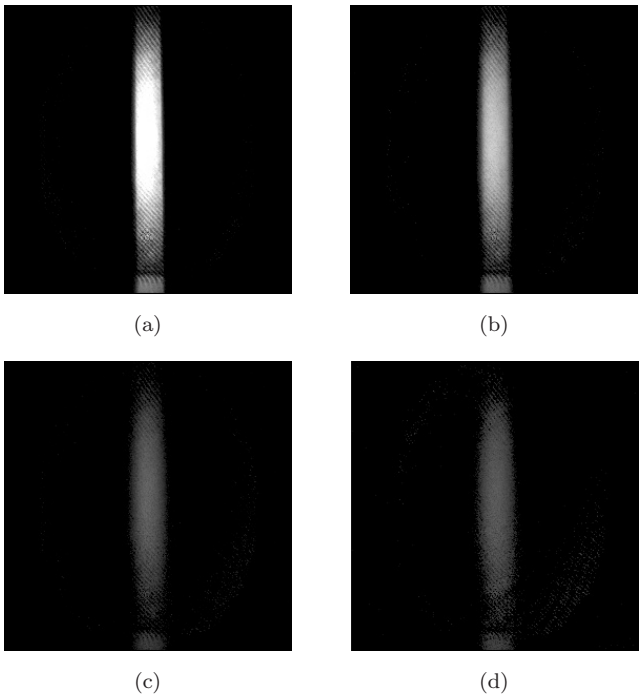

Fig. 5. Liquid crystal based experimental images of the linear dichroism of a linear polarizer located at depths of (a) 2, (b) 5, (c) 10, and (d) 12 mfps within a scattering medium. The images are obtained by combining Figs. 3 and 4. Each image is 8 mm × 8 mm.

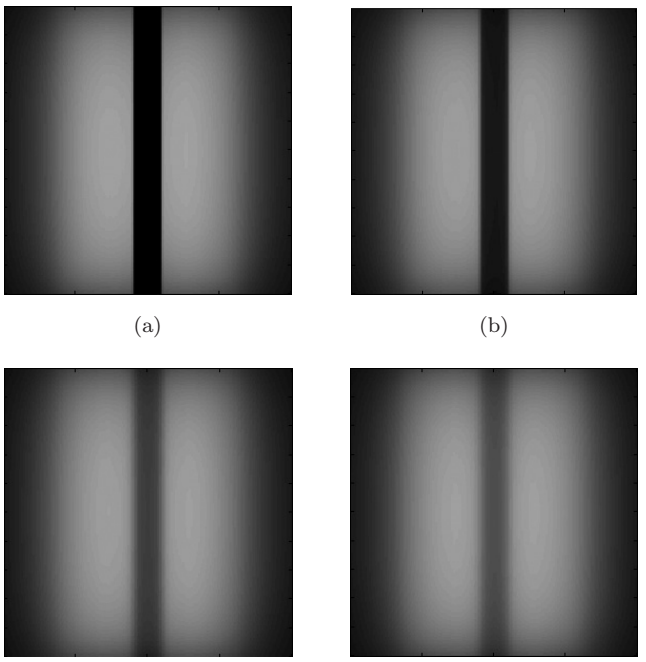

Fig. 6. Monte Carlo simulations of ROPI images of a linear polarizer located at depths of (a) 2, (b) 5, (c) 10, and (d) 12 mfps within a scattering medium. The polarization axis of the target is aligned vertically, the illumination is vertically linearly polarized with horizontal detection. Each image is 200 mfps × 200 mfps.

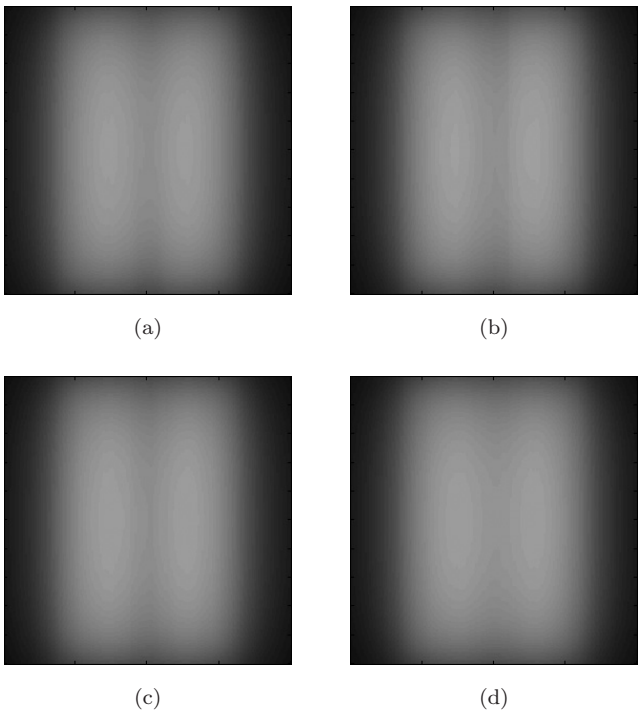

Fig. 7. Monte Carlo simulations of ROPI images of a linear polarizer located at depths of (a) 2, (b) 5, (c) 10, and (d) 12 mfps within a scattering medium. The polarization axis of the target is aligned vertically, the illumination is horizontally linearly polarized with vertical detection. Each image is 200 mfps × 200 mfps.

of target depths (Fig. 9). The error bars in the experimental results represent the spread (standard deviation) of results from repetition of the experiment and the Monte Carlo error bars are obtained from the spread of results from running independent simulations. The increase in size of the error bars with increasing depth is due to a poorer signal to noise ratio. Figure 9(a) shows the calculated dichroism along a central band of 200 pixels in the image. The dichroism values obtained in the Monte Carlo simulation are higher than those obtained with the experiment across the entire depth range. Resolution is defined as the distance that the intensity takes to change from 10 to 90% of the difference between the maximum and minimum values, a low value corresponding to better resolution. The 10–90% distances are lower in the simulation than in the experiment indicating a worse imaging performance in the experiments. Reasons for these discrepancies are discussed in the next section.

4. Discussion and Conclusions

The liquid crystal based system has provided a performance that compares well to that obtained with a previous Glan–Thompson polarizer based

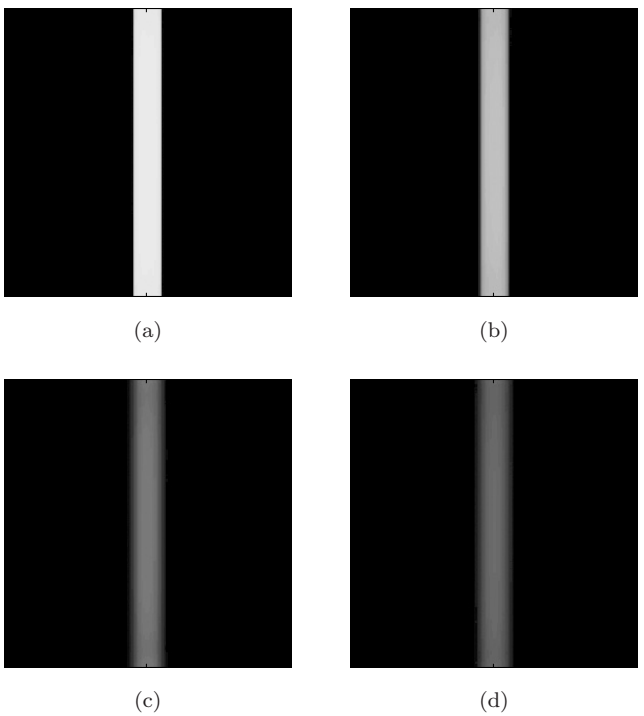

Fig. 8. Monte Carlo simulations of the linear dichroism of a linear polarizer located at depths of (a) 2, (b) 5, (c) 10, and (d) 12 mfps within a scattering medium. The images are obtained by combining Figs. 6 and 7. Each image is 200 mfps × 200 mfps.

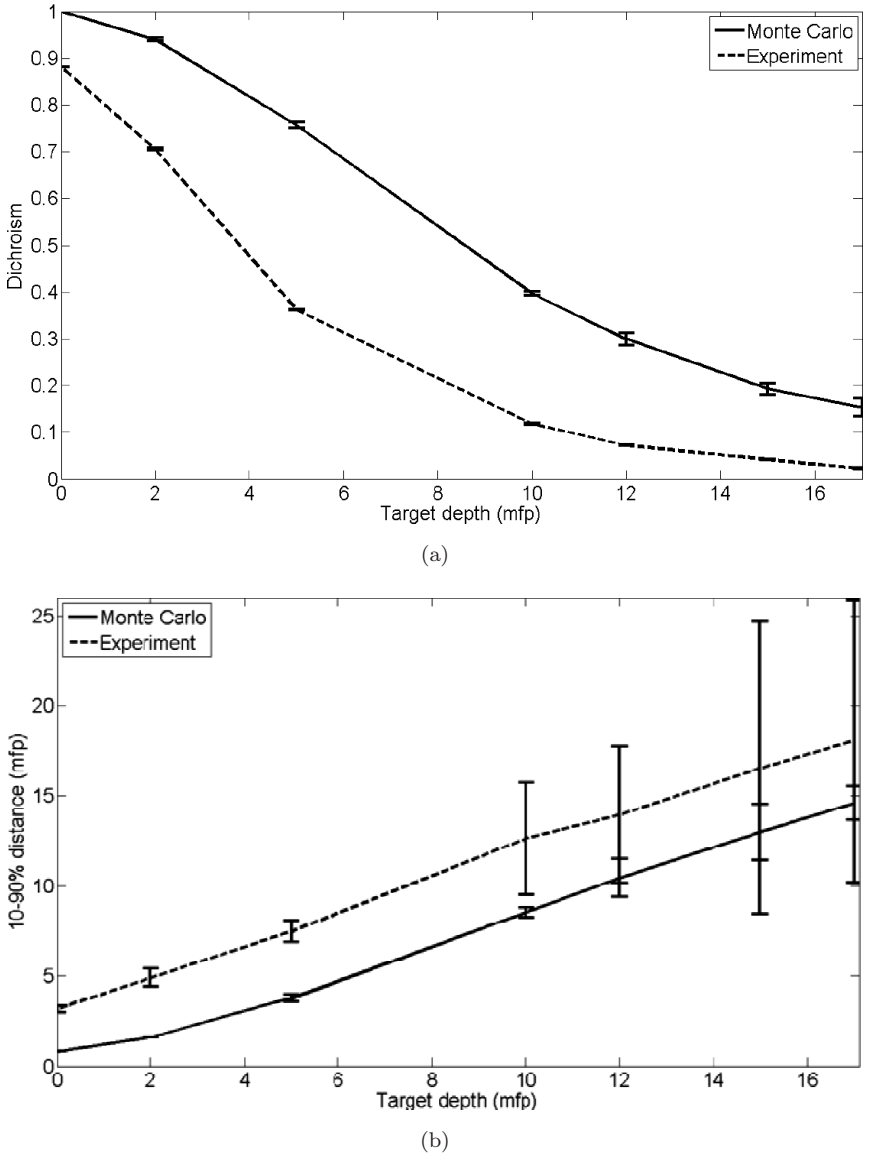

Fig. 9. Comparison of liquid crystal based experimental and simulated polarization difference measurements of a polarizer embedded at different depths within a scattering medium (a) linear dichroism, and (b) resolution defined as the distance taken for the dichroism value to change from 10 to 90% of its maximum value.

system with manual rotation of the polarizers.[1,2] The technique is useful as the presence of linear dichroism can be detected in the presence of significant scattering due to the system utilizing a detection channel that is always orthogonal to the illumination polarization state. Furthermore, the approach rejects reflections from surfaces of the optical components within the system, meaning that co-axial detection can be used. A drawback to the ROPI approach is that the dichroism measurement is depth dependent due to the effects of scattering between the target and detector. It is therefore an important part of future work to investigate whether dichroism and target depth can be decoupled as part of an inversion algorithm. It is likely that multiple wavelengths or utilizing the spatial distribution of the emerging light may be useful additional measurements in making the inversion better conditioned.

The imaging results obtained provide confidence that the liquid crystal based system can replace the system based on manual rotation of the polarizers. The liquid crystal based system is a significant step forward in the development of a robust device that can be taken into the clinic or biology laboratory. This has been demonstrated in microscopy to be an important step forward to the widespread use of a technique. For example,

introducing liquid crystals into a polarized light microscope has resulted in a robust commercial microscope, the LC Polscope.[10]

The Monte Carlo simulation provides results that qualitatively compare well with those obtained in the experiment in terms of dichroism against depth and resolution against depth. There are several assumptions made in the model that cannot be accurately achieved in the experiment such as ideal polarizers, precise depth location of the target, precise alignment of optical components, a refractive index match between the target and surrounding medium, an infinitely long and thin target, and uniform illumination. For the dichroism measurements (Fig. 9(a)) the most likely source of the difference between the experiment and simulation is due to reflections from the surface of the cuvette introducing a contribution into the orthogonal detection channels. This should be completely removed by the analyzer but a small contribution is still detected due to the finite rejection of the polarization optics. For the resolution against depth plot (Fig. 9(b)) the modeling results follow the same trend as the experiment. The main source of the difference between them is the finite thickness of the target which results in the target occupying a range of depths. To better simulate the phantom study further refinements of the model could be performed such as making the polarizers nonideal, the target of finite thickness or introducing surface reflections at the medium-target boundary. At this stage, however, this would greatly increase the complexity of the model and is unlikely to provide any additional insight into the tissue imaging problem.

In conclusion, ROPI has previously been implemented using a Glan–Thompson based system with manual rotation of the polarizers to obtain illumination and analysis of the light. Although the system could be implemented using motorized rotation stages, there are disadvantages in terms of image alignment and ease of use of the system in practical applications. The liquid crystal based system demonstrated in this paper provides an important step forward in making this technique clinically applicable. Moving parts are removed and the imaging performance is comparable to that obtained with previous systems and Monte Carlo simulations.

Acknowledgments

The authors would like to acknowledge support from the Engineering and Physical Sciences Research Council (EP/C534247/1). Q. Zhu was funded by a studentship from the international office at the University of Nottingham.

References

1. S. P. Morgan, Q. Zhu, I. M. Stockford, J. A. Crowe, "Rotating orthogonal polarization imaging," *Opt. Lett.* **33**(13), 1503–1505 (2008).
2. S. P. Morgan, Q. Zhu, I. M. Stockford, J. A. Crowe, "Rotating orthogonal polarization imaging for tissue imaging," *Proc. SPIE* **6858**, 68580A (2008).
3. D. A. Beach, C. Bustamante, K. S. Wells, K. M. Foucar, "Differential polarization imaging. 3. Theory confirmation — patterns of polymerization of haemoglobin-S in red blood sickle cells," *Biophys. J.* **53**, 449–456 (1988).
4. S. P. Morgan, I. M. Stockford, J. A. Crowe, B. R. Hayes-Gill, "Optical imaging and spectroscopy of superficial tissue," *J. Innov. Opt. Health Sci.* **1**, 85–93 (2008).
5. M. Morgan, O. Kostyuk, R. A. Brown, V. Mudera, "*In situ* monitoring of tendon structural changes by elastic scattering spectroscopy: Correlation with changes in collagen fibril diameter and crimp," *Tissue Eng.* **12**, 1821–1831 (2006).
6. R. J. McNichols, G. L. Cote, "Optical glucose sensing in biological fluids: An overview," *J. Biomed. Opt.* **5**, 5–16 (2000).
7. S. L. Jacques, J. R. Roman, K. Lee, "Imaging superficial tissues with polarized light," *Lasers Surg. Med.* **26**, 119–129 (2000).
8. S. P. Morgan, I. M. Stockford, "Surface reflection elimination in polarization imaging of superficial tissue," *Opt. Lett.* **28**, 114–116 (2003).
9. B. Boulbry, T. A. Germer, J. C. Ramella-Roman, "A novel hemispherical spectro-polarimetric scattering instrument for skin lesion imaging," *Proc. SPIE* **6078**, 128–134 (2006).
10. R. Oldenbourg, "Polarization microscopy with the LC-PolScope," in *Live Cell Imaging: A Laboratory Manual*, D. L. Spector, R. D. Goldman, Eds., pp. 205–237, Cold Spring Harbor Laboratory Press, NY (2004).
11. C. F. Bohren, D. R. Huffman, *Absorption and Scattering of Light by Small Particles*, John Wiley & Sons (1983).
12. P. C. Y. Chang, J. G. Walker, K. I. Hopcraft, B. Ablitt, E. Jakeman, "Polarization discrimination for active imaging in scattering media," *Opt. Commun.* **159**, 1–6 (1999).
13. W. S. Bickel and W. M. Bailey, "Stokes vectors, Mueller matrices, and polarized scattered light," *Am. J. Phys.* **53**, 468–478 (1985).